JOURNAL OF SPACECRAFT AND ROCKETS
Vol. 38, No. 2, March–April 2001

Engineering Notes

ENGINEERING NOTES are short manuscripts describing new developments or important results of a preliminary nature. These Notes cannot exceed six manuscript pages and three figures; a page of text may be substituted for a figure and vice versa. After informal review by the editors, they may be published within a few months of the date of receipt. Style requirements are the same as for regular contributions (see inside back cover).

Thermal Characterization of a Direct Gain Solar Thermal Engine

Reginald A. Alexander*
NASA Marshall Space Flight Center, Huntsville, Alabama 35812
and
Hugh W. Coleman†
University of Alabama in Huntsville, Huntsville, Alabama 35899

Introduction

MEANS of producing thrust other than by chemical propulsion are being investigated in efforts to find better and cheaper ways to explore space and insert payloads into Earth orbit. One of these innovative approaches is to use solar energy to produce thrust. A solar thermal engine collects concentrated solar energy, which is used to heat hydrogen propellant to temperatures on the order of 4000–5000°F, and the heated propellant exits at a high velocity through the engine's nozzle, thus producing thrust. The major benefit to using the solar thermal engine is the expected increased specific impulse I_{sp}. This high I_{sp} is due to the low molecular weight of H_2 and the exhaust velocities of the propellant exiting the nozzle. The I_{sp} is proportional to $\sqrt{(T_c/M)}$, where T_c is the propellant chamber (stagnation) temperature and M is the propellant molecular weight.[1] Because H_2 has the lowest molecular weight of any element, increasing the temperature is necessary to increase the I_{sp}. Typical liquid oxygen/liquid hydrogen (LO_2/LH_2) chemical stages have I_{sp} of 436 s, whereas a typical solar thermal upper stage (STUS) design should have an I_{sp} of about 860 s if a fluid temperature of approximately 4100°F could be attained.

The work presented here reports results from the thermal/fluids modeling of a STUS engine designed to produce about 2 lb of thrust, which makes it useful to boost payloads to higher orbits over a long period of time or for satellite station keeping. The models developed were used to calculate the pressure loss in the engine, fluid velocities, and the fluid temperature along the solar thermal absorber up to the nozzle. When this information is used, one can determine the performance of the engine. A sensitivity study was performed to investigate the effects on engine performance of changes in the convection coefficient in the ducts, the hydrogen mass flow rate, the emissivity of the absorber surface, and the insulation thickness.

Solar Thermal Engine Design

The solar thermal engine is shown in Fig. 1. The absorber cavity, which totaled 16.3 in. in length, was a cylinder with a hemispherical end and was made of tungsten (which has a melting point of 5684°F). The diameter at the mouth of the absorber was 2.652 in., whereas the diameter at the end of the cylinder was 2.588 in. The cylindrical portion of the absorber was 15 in. long with the balance being the end cap. The tapering of the cylinder was to aid in the removal of the absorber from the mandrel on which it was sprayed using vacuum plasma spray (VPS) techniques. The H_2 ducts were formed using VPS techniques also. Tungsten was deposited on a mandrel that was threaded such that it produced a helical duct when the mandrel was removed. There were two parallel ducts each having a helical pitch of 1, meaning that one helical revolution of the absorber was completed for every inch of the absorber length. The shell that formed the ducts had an outer diameter of 3.213 in. at the beginning and a diameter of 3.170 in. at the end. The ducts were triangular in cross section with an area of 0.045 in.,[2] base of 0.45 in., and height of 0.21 in. The walls of the ducts and the absorber cavity were 0.08 in. thick. There was a gap of 0.204 in. between the tip of the duct walls and the Fiberform® insulation, designed to operate at temperatures up to 5000°F. The Fiberform insulation facing the ducts had a low-emittance graphite coating, providing a reflective coating effective at high-temperature operation. The entire engine and insulation assembly was enclosed in stainless steel.

The energy used to heat the engine is provided through concentrated solar energy. The solar energy spectral distribution is approximately 7% ultraviolet, 46% visible, and 47% near infrared. The majority of the energy emitted by the sun is at a much shorter wavelength than the infrared energy emitted by a body near the design temperature of the surface of the absorber. This allows for the selection of finishes that are absorbing or reflective in the solar spectrum while performing oppositely at long infrared wavelengths. For an engine of this type, it is desirable to have a high solar absorbtivity and a low emissivity at the temperature of the surface because that would enable more energy to be transferred to the fluid rather than be radiated to the environment. The absorbtivity α is the fraction of energy that is absorbed by a surface compared to the energy absorbed by black surface, $\alpha = 1$, whereas the emissivity ε is the fraction of the energy that is emitted compared to that emitted by a black surface, $\varepsilon = 1$, of the same temperature. The design specification of the engine required that the surface of the first 4 in. of the absorber cavity be polished to have an α of 0.25, while the balance of the absorber would have an α of 0.75 at solar radiation wavelengths, with corresponding infrared wavelength emissivities of 0.1 and 0.22. This was

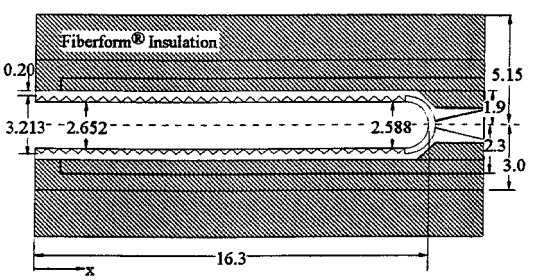

Fig. 1 Schematic of the solar thermal engine. All dimensions are in inches.

Received 15 June 2000; revision received 14 November 2000; accepted for publication 17 December 2000.

*Aerospace Engineer, Vehicle Subsystem Engineering TD52; Reginald.Alexander@msfc.nasa.gov.

†Eminent Scholar in Propulsion and Professor, Propulsion Research Center, Mechanical and Aerospace Engineering Department; coleman@mae.uah.edu. Associate Fellow AIAA.

done in the absorber entrance area to tailor the fluid heating profile by increasing the percentage of the solar flux absorbed deeper in the cavity.

Thermal Model

The cases analyzed assumed 1) that 10 kW of solar energy was concentrated such that it had a half angle of 32 deg as it entered the absorber cavity and 2) that gaseous H_2 was flowing through the absorber at the rate of 2 lb/h for the nominal design. The engine was assumed to be in a vacuum chamber and at an initial temperature of 70°F. No attempt was made to model the nozzle flow or heat transfer in the nozzle area; only the heat transfer and fluid dynamics associated with the absorber, ducts, and the insulation were modeled.

A detailed description of the modeling is given in Ref. 2, and only a brief overview is presented here. The solar thermal engine was modeled using SINDA,[3] and radiation view factors were calculated using TRASYS,[4] which can be used to calculate the internode radiation interchange of a model as well as calculate the incident and absorbed heat rate data from environmental heat sources.

An in-house Monte Carlo simulation code (W. Emrich, NASA Marshall Space Flight Center, personal communication, August 1997) was used to determine the incident energy distribution inside the absorber cavity that was used for input to the analysis. The optical properties for the calculations were values that were integrated over the solar spectrum for the tungsten surface. The code generated random light rays entering the cavity and for each of the rays determined where it struck the surface of the absorber and where its reflections struck until the intensity was only 1% of the original value. The output from the simulation was a normalized distribution of the light on the absorber specific to the optical properties of the absorber and the angle at which it was concentrated. The resulting distribution was given in terms of a ratio $\boldsymbol{R}$ defined by

$$R = \left(\frac{q_{xy}/a_{xy}}{Q_T/A_{\text{mouth}}} \right)$$

where q_{xy} is the rate of energy flow into the area a_{xy} and Q_T is the rate of total energy flow passing through A_{mouth}, the area of the mouth of the absorber. The distribution, shown in Fig. 2, has two peaks at about 2.5 and 5 in. along the absorber cylinder. The first peak is due to the light entering the absorber at a half cone angle of 32 deg and striking the surface and being absorbed. The second peak is caused by the reflections of light from the first region of incidence. Light is reflected farther into the absorber, but it is more evenly distributed on the absorber surface. The peak at the end of the absorber is due to light directly incident on the surface from the source.

Of particular interest in modeling the engine was the temperature of the fluid as it flowed along and exited the absorber. The primary mode of heat transfer to the fluid in the ducts was forced convection, and so the fluids modeling focused on determining the convection coefficients needed to calculate the temperature of the fluid. The pressure loss of the fluid as it flowed through the engine ducts was also of interest. Both of these were complicated by the triangular shape of the ducts and the curvature effects due to the coiled configuration of the ducts. As described in detail in Ref. 2, these effects were taken into account in the model, and the curvature had a significant effect on the value of the convection coefficient in the ducts. For all cases analyzed, the flow was laminar, the Mach number was less than 0.1, and the pressure drop from the duct inlet to the chamber was 5 psi or less.

Results

The transient fluid temperature distribution is shown in Fig. 2, where it is seen that after 30 min of operation the fluid chamber temperature is within about 40°F of the steady-state temperature of 3850°F and that after only 5 min of operation the temperature is within 500°F of steady state. Additional cases were run to investigate the sensitivity of the results from the model to several of the input variables: the convection coefficient in the ducts, the hydrogen mass flow rate, the emissivity of the absorber surface, and the insulation thickness.

Increasing or decreasing the convection coefficient in the ducts by 50% had a negligible effect on the temperature of the fluid at the chamber. This implies that a duct geometry change to attempt to increase h is not worthwhile and also that the effect of the uncertainty in the value of h on the uncertainty in the fluid temperature is negligible.

Similarly, cases were also run in which the emissivity of the absorber surface was increased or decreased by 50%. When rounded numbers are used for ease of comparison, for the nominal case the fluid chamber temperature was 3850°F and 87% of the incident energy went into the fluid. Increasing the emissivity by 50% changed those numbers to 3800°F and 86%, and decreasing the emissivity by 50% changed them to 3900°F and 89%, respectively. Thus, large changes in the emissivity values yield relatively small changes in the performance of the engine, and (as with the convection coefficient) the uncertainty in the value of emissivity has little effect on the uncertainty in calculated fluid temperature.

On the other hand, the fluid chamber temperature is very sensitive to the hydrogen flow rate. Decreasing the flow rate from 2 to 1 lb/h increased the chamber temperature to about 4700°F. Of course, the reduced mass flow rate also would reduce the thrust.

When developing a flight engine the mass and volume occupied are very important. Reducing the insulation thickness of the engine reduces the mass and volume, but also reduces the engine's chamber temperature while increasing the outside shell temperature. Results of the insulation thickness sensitivity analysis (Fig. 3) show that with insulation approximately 0.6 in. thick the steady-state chamber temperature is approximately 3740°F, about 80% of the incident energy goes into the fluid, and the outer shell temperature is about 1000°F. This chamber temperature is only about 100°F less than the chamber temperature of the engine with 3.2 in. of insulation, which has four times the volume of an engine with 0.6 in. of insulation.

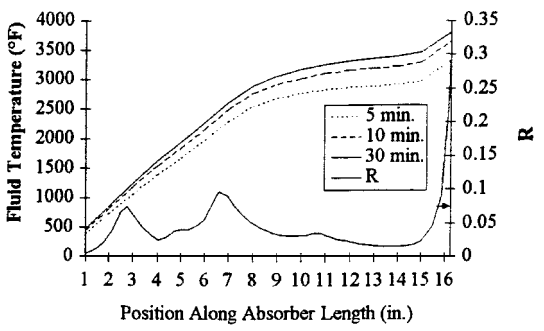

Fig. 2 Incident solar flux distribution and transient fluid temperature distribution.

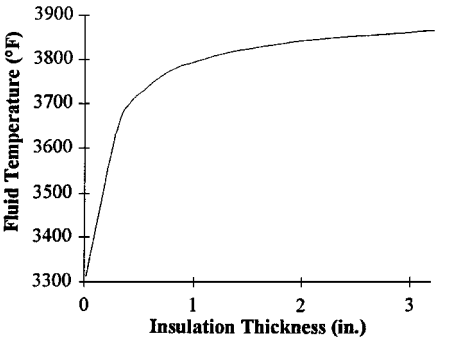

Fig. 3 Steady-state fluid chamber temperature as a function of insulation thickness.

Summary

Results of a thermal analysis of a solar thermal engine showed that the fluid chamber temperature was within 40°F of the steady-state temperature of 3850°F after 30 min of operation, was relatively insensitive to changes in cooling duct convection coefficient and absorber surface emissivity, and was very sensitive to the hydrogen mass flow rate.

References

[1]Strumpf, H. J., Borghese, J. B., and Keating, R. F., "Conical Solar Absorber/Thruster for Space Propulsion," *Solar Engineering*, Vol. 2, American Society of Mechanical Engineers, Fairfield, NJ, 1995, pp 893–902.

[2]Alexander, R. A., "Thermal/Fluids Analysis of a Direct Gain Solar Thermal Upper Stage Engine," M.S. Thesis, Dept. of Mechanical and Aerospace Engineering, Univ. of Alabama, Huntsville, AL, Aug. 1998.

[3]*SINDA/G User's Guide*, 1st ed., Network Analysis Associates, Inc., Fountain Valley, CA, 1994.

[4]"Thermal Radiation Analyzer System (TRASYS) User's Manual," Lockheed Engineering and Management Services Co., Houston, TX, April 1988.

T. C. Lin
Associate Editor

Radiation Exposure Comparison of Venus and Mars Flyby Trajectories

Timothy Crain,* Robert H. Bishop,† and Wallace Fowler‡
University of Texas at Austin, Austin, Texas 78759-5321
and
Kenneth Rock§
Motorola, Leesburg, Virginia 20176

Introduction

FOLLOWING the lead of the Apollo lunar flyby missions that predated Apollo 11, a Venus or Mars flyby mission would serve to verify the ability to sustain astronauts in the interplanetary environment without the additional complexity of a Mars entry and landing. In addition to assessing propulsion and life-support requirements, the mission planner analyzing a trajectory for a crewed Mars transportation and habitation vehicle (TransHab) demonstrator must consider radiation exposure and related hazards. An approximate radiation model has been developed to quantify the radiation hazard of trajectories as a function of time and distance from the sun. Interplanetary spacecraft radiation exposure is approximated by incorporating models for galactic cosmic radiation (GCR) and solar particle events (SPEs). GCR is the ambient radiation experienced from energetic processes of the stars and galaxies outside this solar system. This radiation decreases in intensity with proximity to the sun. SPEs include solar flares and are relatively brief, intense periods of radiation that increase with solar proximity.

Ballistic Earth–Mars–Earth (EME) and Earth–Venus–Earth (EVE) trajectories for the period beginning 1 January 2002 and ending 31 December 2011 have been developed using a hybrid global–local parameter search method.[1] The EVE 2010 and EME 2006 trajectories represented in Fig. 1 were determined to be favorable candidate missions based on their propulsion requirements and time of flight. Risk assessments of the EVE and EME trajectories are given and the Venus flyby trajectory will be shown to be superior to the Mars flyby in terms of radiation exposure.

Received 1 March 2000; revision received 2 June 2000; accepted for publication 2 June 2000.

*Graduate Student, Center for Space Research. Member AIAA.

†Associate Professor, Center for Space Research. Associate Fellow AIAA.

‡Professor, Center for Space Research. Fellow AIAA.

§Orbit Analyst, Satellite Network Operations Center, 44330 Woodridge Parkway.

Table 1 Acute dose effects on humans

Effect	Dose, RAD
Blood-count changes	0–50
10% Chance of vomiting	80–120
25% Chance of vomiting, other symptoms	130–170
50% Chance of vomiting, other symptoms	180–220
20% Chance of death in 2–6 weeks	270–330
50% Chance of death in 1 mo	400–500
Nausea within 4 h, few survivors	550–750
Nausea within 1–2 h, no survivors	1000
Immediate incapacitation	5000

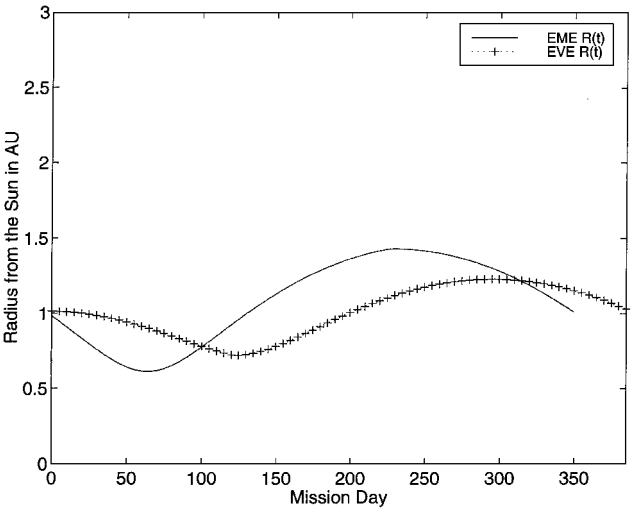

Fig. 1 EME 2006 and EVE 2010 mission radius vs mission day.

Radiation Model

Shielding of humans and equipment from interplanetary radiation can be accomplished in a number of ways: 1) dedicated shielding material in specific locations, 2) efficient and thoughtful placement of inert spacecraft mass, and 3) active magnetic field generation shielding in a manner that emulates the Van Allen belt.[2–4] The model developed here uses a uniform water shield of variable thickness in its calculation of exposure to interplanetary radiation. The interplanetary radiation environment is composed of energies from four sources: 1) radiation emitted from onboard medical equipment, power sources, and propulsion systems; 2) steady-state flux of particles, primarily protons, from the sun, known as the solar wind; 3) low flux radiation (~4 particles/cm^2) of energetic ionized nuclei encountered from the high-energy activity of surrounding stellar bodies known as GCR[5]; and 4) intermittent radiation emitted from the sun during SPEs, such as solar flares and coronal mass ejections.[4]

For the purpose of this study, radiation from onboard sources is assumed to be low level and well shielded for the duration of the times of flight of the EVE and EME mission profiles. The steady-state solar flux is also of a negligible magnitude in comparison with the nominal range of GCR radiation. Thus, only GCR and SPE are considered in connection with potential radiation hazards. The effects of radiation can either manifest immediately from exposure to very high doses or may manifest in the long term from the cumulative doses encountered in an astronaut's career or equipment's operational lifetime. A tentative guideline for human exposure to immediate radiation doses over varying lengths of time in operation of the International Space Station (ISS) is given in Table 1 (Ref. 4). A long-term dose guideline for cumulative exposure limits daily, monthly, and annual roentgen equivalent in man (REM) to 25, 50, and 100–500 units, respectively.[5]

The units of radiation effect in these guidelines are the radiation dose (RAD) and the REM. A RAD is equal to 0.01 J/kg and is used primarily as a material-independent measure of radiation. The REM